Assessing the influence of the rhizosphere on soil hydraulic properties using X-ray Computed Tomography and numerical modelling

Author list: Keith R. Daly[2], Sacha J. Mooney[1], Malcolm J. Bennett[1], Neil M. J. Crout[1], Tiina Roose[2], Saoirse R. Tracy[§1]

Author affiliations:

[1] School of Biosciences, University of Nottingham, Sutton Bonington Campus, Leicestershire, LE12 5RD. United Kingdom.

[2] Bioengineering Sciences Research Group, Faculty of Engineering and Environment, University of Southampton, University Road, Southampton, SO17 1BJ. United Kingdom.

[§] Corresponding author: School of Biosciences, University of Nottingham, Sutton Bonington Campus, Leicestershire, LE12 5RD. United Kingdom, email: saoirse.tracy@nottingham.ac.uk

Short title for page headings: Influence of the rhizosphere on soil hydraulic properties

Short statement: Using non-destructive imaging techniques and numerical modelling we quantify differences in hydraulic and structural properties of bulk and rhizosphere soil for sand and clay loam soils.

1. Abstract

Understanding the dynamics of water distribution in soil is crucial for enhancing our knowledge of managing soil and water resources. The application of X-ray Computed Tomography (CT) to the plant and soil sciences is now well established. However, few studies have utilised the technique for visualising water in soil pore spaces. Here we utilise this method to visualise the water in soil in situ and in three-dimensions at successive reductive matric potentials in bulk and rhizosphere soil. The measurements are combined with numerical modelling to determine the unsaturated hydraulic conductivity, providing a complete picture of the hydraulic properties of the soil. The technique was performed on soil cores that were sampled adjacent to established roots (rhizosphere soil) and from soil that had not been influenced by roots (bulk soil). A water release curve was obtained for the different soil types using measurements of their pore geometries derived from CT imaging and verified using conventional methods e.g. pressure plates. The water, soil and air phases from the images were segmented and quantified using image analysis. The water release characteristics obtained for the contrasting soils showed clear differences in hydraulic properties between rhizosphere and bulk soil, especially in clay soil. The data suggests that soils influenced by roots (rhizosphere soil) are less porous due to increased aggregation when compared to bulk soil. The information and insights obtained on the hydraulic properties of rhizosphere and bulk soil will enhance our understanding of rhizosphere biophysics and improve current water uptake models.

Keywords: Bulk soil; matric potential; rhizosphere; soil pores; water release characteristic; X-ray Computed Tomography; image based homogenisation.

Abbreviations:

(3D) – 3-Dimensional

(CT) - Computed Tomography

(ROI) - Region of Interest

(WRC) – Water Release Characteristic

(WFP) – Water Filled Pores

(AFP) – Air Filled Pores

(REV) - Representative elementary volume

2. Introduction

The concept of the 'rhizosphere', proposed by Hiltner (1904), refers to the volume of soil adjacent to a plant root over which the root has influence. The rhizosphere is created from root-soil-microbe interactions and the compression of soil due to root expansion (Aravena *et al*., 2011; Aravena *et al*., 2014; Dexter, 1987; Whalley *et al*., 2005). Soil physical structure affects root growth, however, in turn a growing root physically alters the soil structure through the creation of biopores (Stirzaker *et al*., 1996), which impact on fluid transport through soil (Angers and Caron, 1998). Root water uptake leads to further soil structural changes through drying which may cause soil shrinkage (Towner and Childs, 1972). The root also secretes chemical compounds, referred to as exudates, into the surrounding soil. These exudates can be divided into three categories: (1) mucilage, which is usually found at the root tips and consists of polysaccharides and uronic acids; (2) molecules excreted by the root hairs such as amino acids, organic acids and simple sugars; and (3) cellular organic substances produced by root epidermis senescence (Tan, 2000). Gases are also released from roots, including carbon dioxide and methane, although some researchers (Grayston *et al*., 1997; Swinnen *et al*., 1995) do not define them as exudates as they diffuse into the atmosphere. Aside from the gases released by roots, the remaining exudates constitute a resource that is highly valued by micro-organisms, resulting in a much greater diversity of micro-organisms in the rhizosphere than in the surrounding bulk soil (Smalla *et al*., 2001). The microbial community that exists in the rhizosphere results in several dynamic processes, some of which aid nutrient cycling and aggregation of soil particles. The release of root exudates into the soil also changes its chemical and physical characteristics which enhances microbial growth (Gregory, 2006).

Soil characteristics within the rhizosphere are thought to be markedly different from the bulk soil. For example, rhizosphere soil has been shown to contain greater numbers of the largest pore sizes (Whalley *et al*., 2005) and is generally more acidic than bulk soil with denitrification being more rapid (Tan, 2000). The hydraulic properties of rhizosphere soil are hypothesised to differ from bulk soil; for example, some root exudates cause hydrophobicity of soil particles which affects their wetting ability (Czarnes *et al*., 2000). In addition, root exudates act like glue by aiding the aggregation of soil particles in the rhizosphere, whilst also decreasing the wetting rate (Czarnes *et al*., 2000; Hallett *et al*., 2009). This stabilising effect is enhanced in dry soil in which the viscosity of root exudates is increased (Walker *et al*., 2003). Root exudates are also important in maintaining root-soil contact in drying soils. As the soil dries, the surface tension of the exudate decreases, increasing its ability to wet surrounding soil particles (Read and Gregory, 1997). Other studies suggest rhizosphere soil may be wetter than bulk soil (Young, 1995) due to the formation of a coherent sheath of soil permeated by mucilage and root hairs, known as the rhizosheath (Gregory, 2006). Small quantities of water are released from the root to the rhizosheath at night while the root absorbs water from the rhizosheath during the day (Walker *et al*., 2003). The rhizosheath therefore has a significant effect on soil hydraulic properties, and roots in general modify the soil structure, affecting the water retention capacity of soil.

In order to investigate the above effects on the hydraulic properties of soil, non-invasive measurements of soil structure are required. There has been significant growth in the use of X-ray Computed Tomography (CT) as a method to non-destructively visualise and quantify water flow in soil (Crestana *et al*., 1985; Mooney, 2002; Mooney *et al*., 2012). Mathematical modelling combined with CT has also been widely used to obtain properties of porous materials based on pore scale geometries (Blunt *et al*., 2013), and to understand the effect of

110 root induced compaction using a Darcy-Richards' formulation (Aravena *et al*., 2011; Aravena
111 *et al*., 2014). Recently, Tracy *et al*., (under revision), combined CT imaging and image based
112 quantification with numerical modelling, (Daly and Roose, 2014; Pavliotis and Stuart, 2008),
113 to calculate the hydraulic conductivity of soil using direct measurements of soil pore structure
114 under a range of different saturation conditions. In this paper we demonstrate the application
115 of this method to quantify water distribution in soil pores for bulk and rhizosphere soil in
116 contrasting soil textures. By combining CT imaging with mathematical modelling and up-
117 scaling techniques we are able to determine the effect of a living root system on shaping the
118 soil structure (i.e. rhizosphere morphology) on the hydraulic and structural properties of soil
119 under a range of different saturation conditions.

120

121 **3. Materials and Methods**

122

123 *3.1. Sample preparation*

124 Soil was obtained from The University of Nottingham farm at Bunny, Nottinghamshire, UK
125 (52.52° N, 1.07° W). The soils used in this study were a Eutric Cambisol (Newport series,
126 loamy sand/sandy loam) and an Argillic Pelosol (Worcester series, clay loam). Particle size
127 analysis for the two soils was: 83% sand, 13% clay, 4% silt for the Newport series and 36%
128 sand, 33% clay, 31% silt for the Worcester series. Typical organic matter contents were 2.3%
129 for the Newport series and 5.5% for the Worcester series (Mooney and Morris, 2008). Loose
130 soil was collected from each site in sample bags, sieved to <2 mm and packed into columns
131 (120 mm height, 60 mm diameter) at a bulk density of 1.2 Mg m^{-3}. The soil was mixed to
132 distribute the different sized soil particles evenly before pouring it in small quantities into the
133 columns. After compacting each layer, the surface was lightly scarified to ensure homogeneous

packing and hydraulic continuity within the column (Lewis and Sjostrom, 2010). The soil columns were saturated slowly by wetting from the base for 12 h and allowed to drain freely for 48 h. All columns were weighed and maintained at this weight throughout the experiment by adding the required volume of water daily to the top of the column to ensure soil moisture content remained near a notional field capacity. Half the columns were planted with a single wheat seed (*cv*. Zebedee) and grown for 4 weeks in a growth room, 16 hr day 8 hr night, day temperature 24ºC, night temperature 18ºC, 50% humidity. At the end of the growth period small soil cores (10 mm height, 10 mm diameter) were carefully excavated from the centre of the soil columns. The columns that contained a plant were considered to have developed a rhizosphere whilst those without were considered to contain only bulk soil. The samples were then CT scanned (see section 3.3). Saturated hydraulic conductivity measurements of all cores were obtained using a constant head device, (Rowell, 1994), for comparison with the model derived values.

3.2. Soil water release characteristic (WRC)

A custom-built vacuum chamber was designed in order to hold the soil sample at a given matric potential whilst undergoing CT scanning as outlined in Tracy *et al*., (under revision). The chamber contained a porous ceramic plate (Soil Moisture Corp, Santa Barbara, CA, U.S.A) on top of which a soil core was placed, with kaolin clay at the base to ensure a good contact. The porous ceramic was first submerged in de-aired water and a vacuum applied to ensure no air bubbles remained trapped within the ceramic. A 0387 Millipore vacuum pump (Merck Millipore, MA, USA) was attached to the chamber and the soil cores were initially saturated before being put under successive vacuums of -5 kPa, -10 kPa, -20 kPa, -40 kPa, -60 kPa and -75 kPa. The vacuum pump was turned on for 120 min then the valve sealed to

158 retain the vacuum inside the chamber. At each successive matric potential the soil core inside
159 the chamber was scanned. After each scan the soil core was removed from the chamber and
160 weighed to calculate water content.

161

162 To obtain a conventional WRC for both soils, a pressure plate Model 1600 Pressure Plate
163 Extractor (Soil Moisture Corp, Santa Barbara, CA, U.S.A) was used. The soil core samples
164 were placed on the plate and weighed frequently until equilibrated at a series of matric
165 potentials. After the final measurement, the samples were oven dried at 105 $^{\circ}$C for 24 hr then
166 weighed.

167

168 *3.3. X-ray Computed Tomography*

169 Three replicate cores from each treatment (bulk or rhizosphere soil) and soil type (sand or
170 clay) of the cores were scanned at the seven matric potentials (0 to -75 kPa) giving a total of
171 84 scans. X-ray CT scanning was performed using a Phoenix Nanotom 180NF (GE Sensing
172 & Inspection Technologies GmbH, Wunstorf, Germany). The scanner consisted of a 180 kV
173 nanofocus X-ray tube fitted with a diamond transmission target and a 5-megapixel (2316 x
174 2316 pixels) flat panel detector (Hamamatsu Photonics KK, Shizuoka, Japan). A maximum
175 X-ray energy of 100 kV and 140 μA was used to scan each soil core. A total of 1440
176 projection images were acquired over a 360° rotation. Each projection was the average of 3
177 images acquired with a detector exposure time of 1 s. The resulting isotropic voxel edge
178 length was 10.17 μm and total scan time was 105 minutes per core. Although much faster
179 scan times are possible it was necessary in this instance to use a longer scan time to acquire
180 the highest quality images to aid with the phase separation of the different soil constitutes.

Two small aluminium and copper reference objects (< 1 mm^2) were attached to the side of the soil core to assist with image calibration and alignment during image analysis. Reconstruction of the projection images to produce 3D volumetric data sets was performed using the software datos|rec (GE Sensing & Inspection Technologies GmbH, Wunstorf, Germany).

The reconstructed CT volumes were visualised and quantified using VG StudioMAX® 2.2 (Volume Graphics GmbH, Heidelberg, Germany). Air, soil and water phases of the scanned volumes were segmented using a threshold technique based on measurements from two reference objects, which were included in each scan, one contained a soil pore water sample and the other finely sieved soil (< 100 μm). The definition of the phases was based on their differences in X-ray attenuation which are represented as greyscale values in the reconstructed CT volumes. This process is described further in Tracy *et al*., (under revision). Image stacks of the extracted volumes for each phase were exported and subsequently analysed for individual pore characteristics using ImageJ v1.42 (http://rsbweb.nih.gov/ij/) (Ferreira and Rasband, 2011). For 2D analysis objects less than two pixels (twice the resolution) in diameter (0.02 mm) and for 3D analysis objects less than two voxels in each direction (8 x 10^{-6} mm^3) were considered as potential noise as a precaution (Wildenschild *et al*., 2005) and subsequently excluded from the analysis.

In order for the geometries of the water-filled pores to be modelled, surface mesh files (.stl) were required; which were generated in VG StudioMax v2.2. After segmentation of the soil water phase, a cube shaped ROI template was imported. Each sample was subsampled, from random initial coordinates, with 6 cubes comprising side lengths of 3.8 mm giving an overall

205 cube volume of $V_m = 54.9\ \mathrm{mm}^3$ (Figure 1). The same coordinates were used for different
206 matric potentials of the same sample.

207

208 *3.4. Numerical modelling*

209

210 To understand the differences between the properties of the rhizosphere and bulk soils we
211 calculate the hydraulic conductivity using the method of homogenization (Pavliotis and
212 Stuart, 2008). This technique enables Darcy's law to be derived from Stokes' equations for
213 fluid flow and, through a mathematically rigorous up-scaling, the hydraulic conductivity to be
214 calculated based on a Representative Elementary Volume (REV). Full details of the scaling
215 and resulting equations can be found in (Daly and Roose, 2014; Hornung, 1997). Further
216 discussion of the assumptions used and their applicability in this context are described in
217 Tracy *et al*., (under revision). Here we summarise underlying assumptions, the method and
218 resulting equations.

219

220 There are several key assumptions that are made in order to develop our model. Firstly we
221 observe that for typical pore sizes the viscous forces dominate the flow properties (Fowler,
222 1997). Hence, we may consider the Stokes limit of the Navier-Stokes equations where all
223 inertial terms are neglected. Secondly, we require that the soil structure is periodic, *i.e*., it is
224 made up of regularly repeating units and, hence, a single one of these units is representative
225 of the overall soil properties. Clearly for real soil samples this is not the case and an apparent,
226 image based, periodicity is enforced by reflection of the REV (Figure 1). The error induced
227 by enforcing periodicity is that the geometry considered numerically is now fully periodic

rather than quazi-periodic and does not truly represent the imaged soil structure. To overcome this, different size REVs were taken from the segmented .stl files. The REVs sampled from the six cubes were of volume, $V = V_m/(2^j)$, where j is a positive integer in the range 0 to 8 such that the smallest volume we consider is $0.2\,\mathrm{mm}^3$ and the largest is V_m. As j is decreased and, hence, the size of the REV is increased, the relative size of the errors induced by the reflection decreases. Similarly as the REV size increases, the hydraulic properties of the subsample will, in principle, converge to the hydraulic properties of the soil. Finally, as we are able to segment the air and water separately from the CT scan image of the soil structure, the fluid dynamics can be greatly simplified. Rather than consider the moving interface between each phase we consider the, relatively slow, flow of water about a fixed interface. We further simplify the equations by assuming that the non-wetting phase, in this case air, is stationary. If this is not the case then the movement of the air effectively lubricates the movement of water resulting in an increase in the hydraulic conductivity. This approach is valid assuming firstly that the pressure gradients are sufficiently low that the interface remains fixed and secondly that the non-wetting phase is not connected and, hence, the trapped non-wetting phase has zero average velocity.

After a rigorous mathematical analysis of Stokes equations we are able to derive Darcy's law which is valid for the bulk or rhizosphere soil and describes fluid driven by an external pressure gradient, see (Daly and Roose, 2014; Hornung, 1997). The average water velocity $\boldsymbol{u}$ is given by

$$\boldsymbol{u} = -\mathcal{K}(\boldsymbol{\nabla} p_0 - \rho g \hat{\boldsymbol{e}}_z), \tag{1}$$

where ρ is the fluid density ($\rho = 10^3 \text{kg m}^{-3}$ in the case of water), $g = 9.8 \text{ m s}^{-2}$ is the acceleration due to gravity, p_0 is the applied pressure and $\mathcal{K}$ is the relative permeability (in the general case a tensor) which has components defined as

$$\mathcal{K}_{jk} = \frac{L_y^2}{\mu} \int_{\Omega_w} \hat{\boldsymbol{e}}_j \cdot \boldsymbol{v}_k^w \, dy. \tag{2}$$

Here $\hat{\boldsymbol{e}}_j$, for $j = x, y, z$ is a unit vector in the j-th direction, μ is the viscosity ($\mu = 10^{-3} \text{kg m}^{-1} s^{-1}$ in the case of water), L_y is the length of the REV and $\boldsymbol{v}_k^w$ is the local velocity. The hydraulic conductivity is defined as the average water velocity driven by gravity. Assuming that the air velocity is slower than the water velocity, local "corrector" velocity $\boldsymbol{v}_k^w$ satisfies the following set of equations which are solved on a single REV a single time to parameterise equation (2),

$$\nabla^2 \boldsymbol{v}_k - \boldsymbol{\nabla} \pi_k = \hat{\boldsymbol{e}}_k, \qquad \boldsymbol{\nabla} \cdot \boldsymbol{v}_k = 0, \qquad \boldsymbol{x} \in \Omega_w, \tag{3a}$$

$$\boldsymbol{v}_k = 0, \qquad \boldsymbol{x} \in \Gamma, \tag{3b}$$

$$\pi_k = 0, \ \frac{\partial}{\partial x_k}(\hat{\boldsymbol{e}}_k \cdot \boldsymbol{v}_k) = 0, \ \hat{\boldsymbol{e}}_j \cdot \boldsymbol{v}_k = 0, j \neq k \qquad \boldsymbol{x} \in \Gamma x_k \tag{3c}$$

$$\frac{\partial \pi_k}{\partial x_j} = 0, \ \frac{\partial}{\partial x_p}\left(\hat{\boldsymbol{e}}_p \cdot \boldsymbol{v}_k\right) = 0, \hat{\boldsymbol{e}}_j \cdot \boldsymbol{v}_k = 0, p \neq k, , p \neq j \qquad \boldsymbol{x} \in \Gamma x_j \tag{3d}$$

where π_k is the local pressure correction due to the microscale geometry, Ω_w is the water domain, Γx_k is the boundary located at $x_k = 0$, $x_k = 1/2$, Γx_j is the union of the boundaries located at $x_j = 0$ and $x_j = 1/2$ for $j \neq k$ and Γ is the union of the soil-water interface and the air-water interface (Figure 1). Physically this problem in equations (3a)-(3d) can be thought of as calculating the fluid velocity subject to a unit pressure gradient in direction of $\hat{\boldsymbol{e}}_k$. As

264 the equations are linear Darcy's law follows by multiplying the resulting solution by the
265 pressure gradient.

266

267 Equations (3) were solved numerically on each subsample obtained from the CT images. The
268 equations were solved using OpenFOAM, an open source Computational Fluid Dynamics
269 toolbox running on IRIDIS, the High Performance Computing Facility at the University of
270 Southampton. The result is a set of hydraulic conductivity calculations that converge to the
271 true hydraulic conductivity of the soil, at each point along the WRC, as the sub-volume size
272 is increased.

273

274 To further quantify the results we have fitted the van Genuchten model for the WRC and the
275 unsaturated hydraulic conductivity (van Genuchten, 1980) to the calculated values using a
276 non-linear least squares method. The volumetric water content θ is given by

$$\theta = (\theta_s - \theta_r)\left(\frac{1}{1+(\alpha h)^n}\right)^m + \theta_r, \tag{4}$$

277 where θ_s and θ_r are the saturated and residual volumetric water content respectivel, h is the is
278 the hydraulic head, $m = 1 - 1/n$ and n and α are the van Genuchten parameters. The
279 corresponding hydraulic conductivity is given by $K = K_{sat} k_r^{vg}$. Here K_{sat} is the saturated
280 hydraulic conductivity and the relative hydraulic conductivity is given by

$$k_r^{vg} = \frac{\{1-(\alpha h)^{n-1}[1+(\alpha h)^n]^{-m}\}^2}{[1+(\alpha h)^n]^{m/2}}. \tag{5}$$

281 We take θ_r to be negligible and fit the remaining parameters to the imaged data.

282

3.5. Statistical analysis

The results obtained directly from the CT images were analysed by general analysis of variance (ANOVA) containing soil type and matric potential and all possible interactions as explanatory variables using Genstat 15.1 (VSN International, UK). The probability of significance P, with a threshold value of ($P<0.05$), corresponding to a 95% confidence limit, was calculated and is used as a measure of significance of results obtained.

4. Results & Discussion

4.1. Hydraulic properties

The WRC was obtained via conventional methods and the imaging method (Figure 2) for bulk and rhizosphere soil in the two soil textures. Despite the differences between the methods the image-based approach does capture the differences between the bulk and rhizosphere soils. For both soil types more water is retained in the bulk soil than within the rhizosphere (Figure 2). Measured in the conventional way this trend is observable for both the sand and clay soils. However, using the imaging method, only the clay soil shows significant difference between the bulk and rhizosphere soils. In general the imaging method provides a good estimate of the volumetric water content at 0 kPa. The method performs less well and provides a noticeable overestimate at more negative matric potentials, compared to the conventional method. The result is that the slope of the WRC with matric potential, which is a key parameter in Darcy-Richards' flow models (Hornung, 1997), is underestimated.

306

307 From the conventionally measured WRC we see that the bulk clay soil responded the least to
308 a decrease in matric potential (Figure 2). The volumetric water content at saturation was high
309 and the soil retained the majority of this water across the matric potential range. The
310 rhizosphere clay soil behaved similarly to the bulk clay soil. However, the initial drainage of
311 the soil from saturation to -30 kPa was much steeper and the resulting volumetric water
312 content was lower compared to the bulk clay soil. The sand soils drained to lower volumetric
313 water contents compared to the clay soils (Figure 2). The rhizosphere sand responded
314 strongly to the decreased matric potential, losing almost half of its water content by -30 kPa.
315 The bulk sand showed an initial lag in drainage, however by -30 kPa the volumetric water
316 content was similar to that of rhizosphere sand. It would appear that the bulk sand soil
317 required a slightly lower matric potential (>-10 kPa) for drainage to occur compared to
318 rhizosphere sand. The differences observed in the WRC between the bulk and rhizosphere
319 soils were most significant for matric potentials < -10 kPa for the sand soil and -20 kPa for
320 the clay soil. Hence, there is significant difference between the behaviour of the different soil
321 types at -30 kPa, a typical field capacity (Richards and Weaver, 1944). These trends are also
322 observed in the imaged data (Figure 2) although the differences between the different soils
323 are less significant.

324

325 The trends in the WRC are supported in the hydraulic conductivity predictions (Figure 3).
326 For all soils the value of the hydraulic conductivity is seen to approximately converge to a
327 fixed value as the REV size is increased (Figures 4 & 5). We note that the negative values
328 obtained for low REV size in Figure 5 do not correspond to a negative hydraulic
329 conductivity. Rather these values tell us that with a REV this small the average hydraulic

conductivity is smaller than the standard deviation and there is no correlation between the values obtained. As the size of the REV is increased the correlation increases and all values become positive. The predicted hydraulic conductivity values are seen to compare with reasonable accuracy to the measured value at 0 kPa (Table 1). Here there is a significant difference observed between the bulk and rhizosphere hydraulic conductivities for the clay soil and relatively little difference for the sand soil. The sizable error bars in these figures are attributed to natural variation in the soil samples that can occur even in repacked soil samples. Despite these variations it is clear that there is a measurable difference between the calculated hydraulic conductivity of the bulk and rhizosphere soils. The calculated hydraulic conductivity for the bulk clay soil is quite high and corresponds to a high number of macropores and cracks (Figures 6 & 7). It is here that the differences in bulk and rhizosphere soil can be most clearly observed as the rhizosphere clay soil has the lowest hydraulic conductivity of the soils considered. In the clay soil a bimodal distribution of pores was observed after successive wetting and drying cycles (Peng *et al*., 2007), the pore sizes consist of a large number of sub-resolution micropores and a smaller number of large cracks and macropores (Figure 6). The large reduction in hydraulic conductivity seen in the clay soil is related to a reduction in the diameter of the pores which contribute significantly to the hydraulic conductivity as the soil drains. This supports the hypothesis that one of the main effects of root exudates is to aid aggregation, reducing the overall macroporosity. In the case of the sand soil there is a wider range of pore sizes. Hence, the impact of the root system has a significantly smaller effect on the overall soil pore size range. In summary, the macroporosity may decrease but, due to the wider range of pore sizes, this has less effect on the overall hydraulic conductivity. Alternatively, the main differences in soil structure may be occurring below the resolution of the CT images.

We fitted the van Genuchten curves to the calculated hydraulic conductivity (Figure 3) and the imaged WRC (Figure 2). The resulting parameter values are given in Table 1. The curves are seen to fit the hydraulic conductivity well for all cases. The WRC fit is less favourable with the slope of the van Genuchten curves for both the sand and clay being under predicted. In the case of the clay soil the comparison is reasonable with a slight under prediction of the volumetric water content at low matric potentials. However, in the case of the sand soil the fit is less good. This suggests that there may be significant sub resolution processes occurring which we are unable to detect.

The results indicate that sand soil responded to the change in pore water pressure more than the associated clay soil, leading to a reduced volumetric water content compared to clay soil. Whilst the differences were not as great as expected this trend could be predicted due to the dominant particle size for the respective soils, *i.e.*, the water in the clay soil is retained in the predominantly smaller pores. The clearest difference observed from the WRC, measured in the conventional way, was the variation in drainage between the bulk and rhizosphere soils. The presence of a higher percentage of clay in the clay soil meant the soil structure is more prone to structural change e.g. shrinkage as the soil drained. Hence, the reason for the greater difference in the clay soil between the bulk and rhizosphere soil may be that the additions of root exudates and possible enhanced microbial activity in the rhizosphere soil intensified the aggregate formation process (Helliwell *et al.*, 2014). We may not have seen this effect as strongly in the sand soil, as this soil only had an average clay content of 13% and previous research suggests a >12% clay content is required for aggregate formation in natural soils (Horn and Smucker, 2005). This result highlights that any 'rhizosphere effect' may be exhibited more strongly in soils with a high clay content and illustrates the requirement for studies that utilise contrasting soil textures as the majority of previous bulk and rhizosphere

work focussed on a single soil texture (Czarnes *et al*., 2000; Smalla *et al*., 2001; Whalley *et al*., 2005). As the clay soil exhibited large scale changes in both porosity and volumetric water content there must be significant large scale structural changes occurring brought about by the rhizosphere. The data suggests that, in the clay soil, the main effect of the root is to reduce the porosity through densification (Dexter, 1988), (Figure 6) and decrease the rate of drainage (Figure 2). In the sand soil the main observed difference is an increase in drainage (Figure 2), with little observable effect on the hydraulic conductivity. This suggests that, in addition to the increased aggregation in the clay soil, additional effects are occurring in the rhizosphere to alter the ability of the soil to retain water.

4.2. Soil pore characteristics

In order to quantify the global air and water content per sample by imaging we define Air Filled Pores (AFPs) and WFPs as single connected regions of air or water respectively. We also define the pore space as the union of all the AFPs and WFPs. In addition we refer to individual pores within the soil as simple connected pathways between two distinct points within the pore space. Typically, the pore space contained a single large WFP that contains over 50% of the water within the pore space and a large number of much smaller AFPs and WFPs. The connected WFPs are the main contributor to both the WRC and the hydraulic conductivity calculations and the WFP volume is analogous to the volumetric water content (Figure 2). However, further insight may be gained into the wetting and drying behaviour of the soils by considering the properties of the AFPs and the total WFP surface area.

403 The water filled porosity decreased with decreasing matric potential (Figures 2 & 7;
404 $P<0.001$). There were no significant differences between total WFP in bulk and rhizosphere
405 soil for both soil types. Previous work by Whalley *et al*. (2005) found that bulk and
406 rhizosphere soils had similar porosities, but contrasting structures, which altered the water
407 retention characteristics. The overall proportion of WFP space reduced by a total of 14% in
408 bulk clay, 26% in bulk sand, 16% in rhizosphere clay and 30% in rhizosphere sand soil from
409 0 to -75 kPa. The total volume of AFP space increased significantly (Figures 7 & 8; $P<0.001$)
410 with decreasing matric potential from saturation (0 kPa). The rhizosphere soil contained
411 larger quantities of AFPs (82.3 mm^3) compared to bulk soil (69.5 mm^3), but the difference
412 was not significant. At 0 kPa the average AFP volume was 45 mm^3 for clay and 51 mm^3 for
413 sand, this increased to just 87 mm^3 in clay and 101 mm^3 in sand (Figure 8; $P<0.001$). There
414 were no significant differences between the average volumes of the individual AFPs at the
415 different matric potentials or soil types.

416

417 The total surface area of the WFPs generally increased as matric potential decreased (Figure
418 8; $P<0.001$). This trend was observed for all treatments. Rhizosphere soil had a greater total
419 WFP surface area (1804 mm^2) compared to bulk soil (1616 mm^2), although the difference
420 was not significant. The total WFP surface area was 1618 mm^2 in bulk clay and 2079 mm^2 in
421 rhizosphere clay, 1615 mm^2 in bulk sand and 1529 mm^2 in rhizosphere sand. Although the
422 total volume of WFPs decreased as matric potential decreased (Figure 2) the surface area
423 increased across successive draining (until -60 kPa). Hence, as the size of the WFPs
424 decreased due to drainage they remained adhesively attached to the soil interface forming
425 thin connected films of water that facilitated flow throughout the pore space. This would have
426 biological advantages to the growing root system as the surface area available for water
427 uptake remains high, although water quantities are reduced (Hillel, 1998). This may sustain a

428 growing plant in short term dry spells between rainfall events (Hunt, 2007). The total surface
429 area of AFPs also increased with decreasing matric potential (Figure 8; $P<0.001$). There were
430 no significant differences between soil types (sand and clay soil) for the surface area of AFPs,
431 but the interaction between soil category (bulk and rhizosphere soil) and matric potential was
432 significant ($P<0.01$). Specifically, the bulk soil AFP space at 0 kPa has a much smaller total
433 surface area (156 mm^2) compared to rhizosphere soil (373 mm^2). As the soil dried to -75 kPa,
434 the resulting AFP space greatly increased to 354 mm^2 (56% increase) in bulk soil and to 373
435 mm^2 (34 % increase) in rhizosphere soil. The average surface area for AFP was larger in the
436 sand (0.0171 mm^2) compared to the clay (0.0168 mm^2).

437

438

439 **5. Conclusions**

440 Here we have used a combination of traditional and novel image based techniques to
441 investigate the effect of rhizosphere formation on soil hydraulic properties. The latter
442 technique employed CT and image based modelling using homogenization theory. This has
443 the main advantage that it provides a method that can be used to derive Darcy's law and the
444 corresponding unsaturated hydraulic conductivity through a representative cell problem. The
445 image-based method was also shown to capture the salient features of the WRC including the
446 pore size and connectivity, which could be viewed and quantified in 3D across the successive
447 drying matric potentials, therefore providing geometrical detail not possible by other
448 methods. However, the image-based method tends to overestimate the volumetric water
449 content at lower matric potentials, which can be attributed to possible partial volume effects
450 and the chosen image resolution. As the matric potential is made increasingly negative, the
451 water saturation decreases and the majority of water is trapped in smaller pores. Once these

452 pores become comparable to or smaller than the resolution of the imaging technique it is
453 impossible to distinguish the difference between air and water and the method becomes less
454 reliable. This trend is observable in both the image based WRC and the unsaturated hydraulic
455 conductivity. Higher resolutions are achievable by X-ray CT than used in this study although
456 this comes at the expense of smaller sample sizes. As this is also not desirable, a trade off
457 must be made between sample sizes and image resolution. Hence, a more favourable
458 comparison between the imaging and conventional methods could be obtained through high
459 resolution imaging of specific regions of interest.

460

461 We observed a decrease in the ability of the rhizosphere to retain water, *i.e.*, the volumetric
462 water content of the rhizosphere is lower than the bulk soil. When the rhizosphere forms the
463 hydraulic conductivity is seen to significantly decrease as the volumetric water content also
464 decreases. This suggests that rhizosphere formation acts to reduce the soil macroporosity
465 through densification of soil by root action, although this was soil texture dependant
466 (Aravena *et al*., 2011; Aravena *et al*., 2014; Dexter, 1987; Whalley *et al*., 2005). This
467 rearrangement of pore geometries by the active root system is likely to have significant
468 implications for key processes such as water and nutrient uptake. These results provide
469 insight into the formation of the rhizosphere in contrasting soil types. Combining this with
470 improved numerical models which capture the dynamics of the fluid-fluid interface and
471 advanced upscaling techniques will provide a much more detailed picture of air and water
472 movement in soil. The information and insights obtained on the hydraulic properties of
473 rhizosphere and bulk soil in contrasting soil textures will enhance our understanding of
474 rhizosphere biophysics and provide the means to improve current and future water uptake
475 models.

476

6. Acknowledgements

478

479 The authors acknowledge the use of the IRIDIS High Performance Computing Facility, and
480 associated support services at the University of Southampton, in the completion of this work.
481 This project was funded by BBSRC BB/J000868/1, a collaborative project between
482 Southampton and Nottingham, PI and overall lead Roose.

483

7. References

485 **Angers D, Caron J**. 1998. Plant-induced changes in soil structure: Processes and feedbacks.
486 In: Van Breemen N, ed. *Plant-induced soil changes: Processes and feedbacks*, Vol. 4:
487 Springer Netherlands, 55-72.
488 **Aravena JE, Berli M, Ghezzehei TA, Tyler SW**. 2011. Effects of Root-Induced
489 Compaction on Rhizosphere Hydraulic Properties - X-ray Microtomography Imaging and
490 Numerical Simulations. *Environmental Science & Technology* **45**, 425-431.
491 **Aravena JE, Berli M, Ruiz S, Suárez F, Ghezzehei TA, Tyler SW**. 2014. Quantifying
492 coupled deformation and water flow in the rhizosphere using X-ray microtomography and
493 numerical simulations. *Plant and Soil* **376**, 95-110.
494 **Blunt MJ, Bijeljic B, Dong H, Gharbi O, Iglauer S, Mostaghimi P, Paluszny A, Pentland**
495 **C**. 2013. Pore-scale imaging and modelling. *Advances in Water Resources* **51**, 197-216.
496 **Crestana S, Mascarenhas S, Pozzi-Mucelli R**. 1985. Static and dynamic three-dimensional
497 studies of water in soil using computed tomographic scanning *Soil science* **140**, 326-332.
498 **Czarnes S, Hallett PD, Bengough AG, Young IM**. 2000. Root- and microbial-derived
499 mucilages affect soil structure and water transport. *European Journal of Soil Science* **51**, 435-
500 443.
501 **Daly KR, Roose T**. 2014. Multiscale modelling of hydraulic conductivity in vuggy porous
502 media. *Proceedings of the Royal Society A: Mathematical, Physical and Engineering Science*
503 **470**.
504 **Dexter AR**. 1987. Compression of soil around roots. *Plant and Soil* **97**, 401-406.
505 **Dexter AR**. 1988. Advances in characterization of soil structure. *Soil and Tillage Research*
506 **11**, 199-238.
507 **Ferreira TAWR, Rasband W**. 2011. The ImageJ User Guide, Version 1.45.,
508 (http://rsbweb.nih.gov/ij/docs/user-guide.pdf).
509 **Fowler AC**. 1997. *Mathematical models in the applied sciences*. U.K: Cambridge University
510 Press.
511 **Grayston SJ, Vaughan D, Jones D**. 1997. Rhizosphere carbon flow in trees, in comparison
512 with annual plants: The importance of root exudation and its impact on microbial activity and
513 nutrient availability. *Applied Soil Ecology* **5**, 29-56.

514 **Gregory PJ**. 2006. Roots, rhizosphere and soil: the route to a better understanding of soil
515 science? *European Journal of Soil Science* **57**, 2-12.
516 **Hallett P, Feeney D, Bengough A, Rillig M, Scrimgeour C, Young I**. 2009. Disentangling
517 the impact of AM fungi versus roots on soil structure and water transport. *Plant and Soil* **314**,
518 183-196.
519 **Helliwell JR, Miller AJ, Whalley WR, Mooney SJ, Sturrock CJ**. 2014. Quantifying the
520 impact of microbes on soil structural development and behaviour in wet soils. *Soil Biology*
521 *and Biochemistry* **74**, 138-147.
522 **Hillel D**. 1998. *Environmental Soil Physics*. San Diego Academic Press.
523 **Hiltner L**. 1904. Ueber neuere Erfahrungen und Probleme auf dem Gebiete der
524 Bodenbakteriologie unter besonderer Beruecksichtigung der Gruenduengung und Brache. .
525 *Arb. d. Dtsch.* **Landwirtschaftl. Gesellschaft**, 59–78.
526 **Horn R, Smucker A**. 2005. Structure formation and its consequences for gas and water
527 transport in unsaturated arable and forest soils. *Soil and Tillage Research* **82**, 5-14.
528 **Hornung U**. 1997. *Homogenization and porous media*. Berlin, Germany: Springer.
529 **Hunt CE**. 2007. *Thirsty planet: Strategies for sustainable water management*: Academic
530 Foundation.
531 **Lewis J, Sjostrom J**. 2010. Optimizing the experimental design of soil columns in saturated
532 and unsaturated transport experiments. *Journal of Contaminant Hydrology* **115**, 1-13.
533 **Mooney SJ**. 2002. Three-dimensional visualization and quantification of soil macroporosity
534 and water flow patterns using computed tomography. *Soil Use and Management* **18**, 142-151.
535 **Mooney SJ, Morris C**. 2008. A morphological approach to understanding preferential flow
536 using image analysis with dye tracers and X-ray Computed Tomography. *CATENA* **73**, 204-
537 211.
538 **Mooney SJ, Pridmore TP, Helliwell J, Bennett MJ**. 2012. Developing X-ray Computed
539 Tomography to non-invasively image 3-D root systems architecture in soil. *Plant and Soil*
540 **352**, 1-22.
541 **Pavliotis G, Stuart A**. 2008. *Multiscale Methods: Averaging and Homogenization*: Springer.
542 **Peng X, Horn R, Smucker A**. 2007. Pore Shrinkage Dependency of Inorganic and Organic
543 Soils on Wetting and Drying Cycles *Soil Sci. Soc. Am. J.* **71**, 1095-1104.
544 **Read DB, Gregory PJ**. 1997. Surface tension and viscosity of axenic maize and lupin root
545 mucilages. *New Phytologist* **137**, 623-628.
546 **Richards L, Weaver L**. 1944. Moisture retention by some irrigated soils as related to soil
547 moisture tension. *J. agric. Res* **69**, 215-235.
548 **Rowell DL**. 1994. *Soil science : methods and applications* Longman Scientific & Technical ;
549 Prentice Hall.
550 **Smalla K, Wieland G, Buchner A, Zock A, Parzy J, Kaiser S, Roskot N, Heuer H, Berg**
551 **G**. 2001. Bulk and Rhizosphere Soil Bacterial Communities Studied by Denaturing Gradient
552 Gel Electrophoresis: Plant-Dependent Enrichment and Seasonal Shifts Revealed. *Applied and*
553 *Environmental Microbiology* **67**, 4742-4751.
554 **Stirzaker RJ, Passioura JB, Wilms Y**. 1996. Soil structure and plant growth: Impact of bulk
555 density and biopores. *Plant and Soil* **185**, 151-162.
556 **Swinnen J, Vanveen JA, Merckx R**. 1995. Carbon Fluxes in the Rhizosphere of Winter-
557 Wheat and Spring Barley with Conventional Vs Integrated Farming. *Soil Biology &*
558 *Biochemistry* **27**, 811-820.
559 **Tan KH**. 2000. *Environmental Soil Science* New York: Marcel Dekker, Inc.
560 **Towner GD, Childs EC**. 1972. The mechanical strength of unsaturated porous granular
561 material *Journal of Soil Science* **23**, 481-498.

Tracy S, Daly K, Sturrock C, Crout N, Mooney S, Roose T. 2014. Three dimensional quantification of soil hydraulic properties using X-ray Computed Tomography and image based modelling *Water Resources Research*.
van Genuchten MT. 1980. A Closed-form Equation for Predicting the Hydraulic Conductivity of Unsaturated Soils1. *Soil Sci. Soc. Am. J.* **44**, 892-898.
Walker TS, Bais HP, Grotewold E, Vivanco JM. 2003. Root exudation and rhizosphere biology. *Plant Physiology* **132**, 44-51.
Whalley WR, Riseley B, Leeds-Harrison PB, Bird NRA, Leech PK, Adderley WP. 2005. Structural differences between bulk and rhizosphere soil. *European Journal of Soil Science* **56**, 353-360.
Wildenschild D, Hopmans JW, Rivers ML, Kent AJR. 2005. Quantitative Analysis of Flow Processes in a Sand Using Synchrotron-Based X-ray Microtomography. *Vadose Zone J.* **4**, 112-126.
Young IM. 1995. Variation in moisture contents between bulk soil and the rhizosheath of wheat (Triticum-aestivum L cv Wembley). . *New Phytologist* **130**, 135-139.

List of Tables:

Table 1: Calculated and measured saturated hydraulic conductivity values and the van Genuchten parameters used to fit the calculated data.

585 **Table 1.**

Soil	**Measured K_{sat} $[cm\ s^{-1}]$**	**Calculated K_{sat} $[cm\ s^{-1}]$**	**Saturated volumetric water content θ_s**	**α $[cm^{-1}]$**	**n**
Bulk Sand	0.00225	0.00215	0.458	0.052	1.65
Rhizosphere Sand	0.00276	0.00246	0.450	0.064	1.77
Bulk Clay	0.00208	0.00321	0.494	0.032	1.75
Rhizosphere Clay	0.00136	0.00109	0.446	0.051	1.98

586

587

Figure legends:

Figure. 1: Schematic showing (a) subsampling of segmented volume, (b) subsampled geometry with boundaries Γ_{x_k}, Γ_{x_j} and Γ for $k = 1$, (c) the resulting truly periodic geometry created by reflection of the subsampled region in the x, y and z axis, and (d) typical solution to cell problem showing absolute velocity.

Figure. 2: Water release characteristic of the sand and clay bulk and rhizosphere soils for the conventional and imaging methods.

Figure. 3: Calculated hydraulic conductivity values for clay and sand soils. Data is plotted for bulk and rhizosphere soils and a van Genuchten curve has been fitted through this data using a non-linear least squares method. The parameters are given in table 1.

Figure. 4: Convergence plots for clay soil. For each case (rhizosphere and bulk) three samples were taken. From each of these 6 subsamples were obtained. These plots show the average and standard deviation over the 18 subsamples for increasing subsample size.

Figure. 5: Convergence plots for sand soil. For each case (rhizosphere and bulk) three samples were taken. From each of these 6 subsamples were obtained. These plots show the average and standard deviation over the 18 subsamples for increasing subsample size.

F**igure. 6:** Greyscale images of bulk sand (a), clay (b) and rhizosphere sand (c) and clay (d) soils. Annotations highlight the presence of macropores in sand soil and crack formation in the clay. Scale bar = 2.5 mm.

Figure. 7: 3D core sections of sand and clay, bulk and rhizosphere soil samples at the matric potentials 0 and -75 kPa. Segmented phases are coloured brown (soil), blue (water filled pores) and black (air filled pores). Scale bar = 5 mm.

Figure. 8: Total AFP volume for clay (a) and sand (b) soil, average AFP volume for clay (c) and sand (d) soil, total WFP surface area for clay (e) and sand (f) soil and total AFP surface area values for clay (g) and sand (h) soil at the specific matric potentials. Error bars associated with histograms show one standard deviation.

618 **Figure 1.**

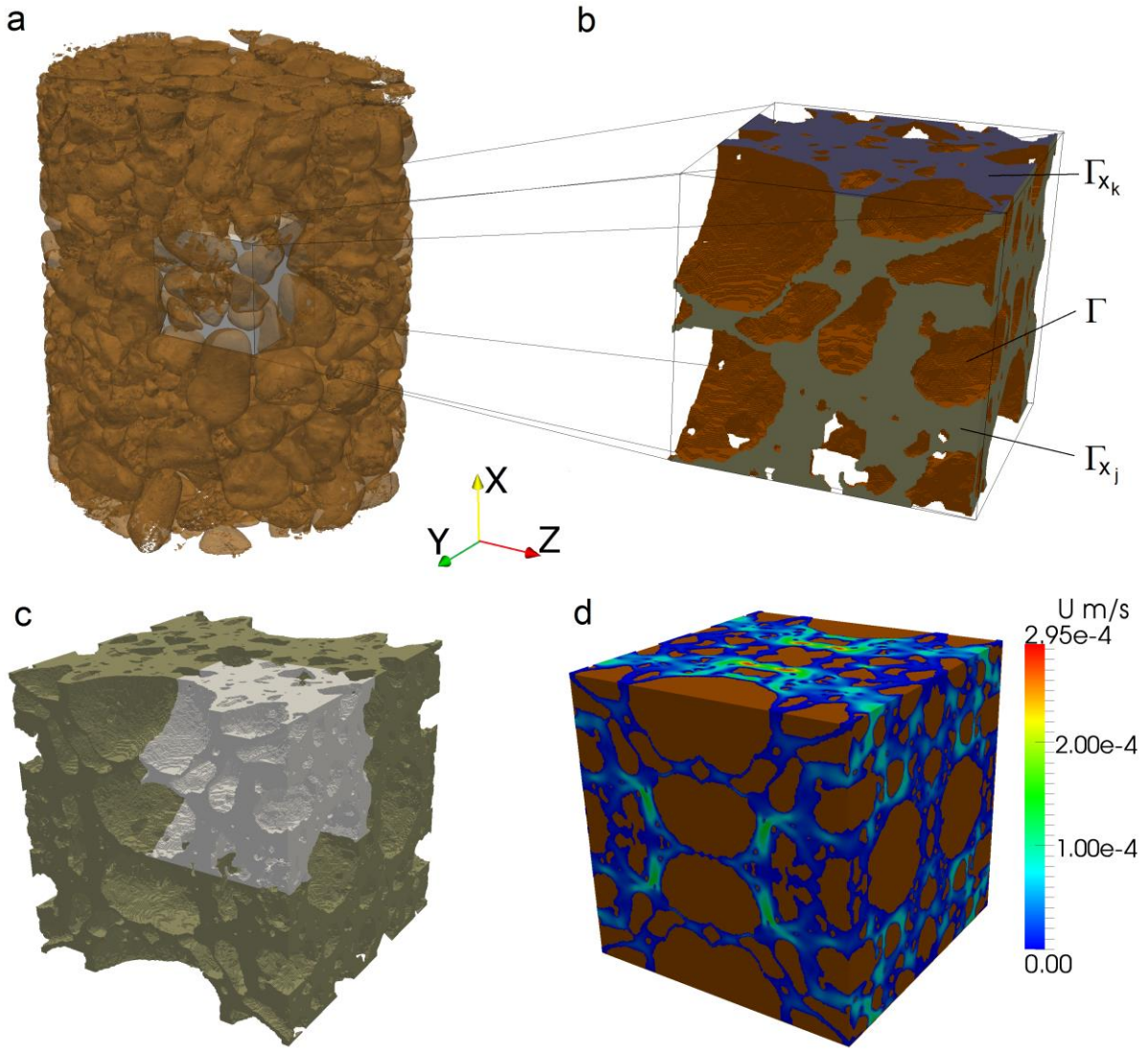

619
620

621 **Figure. 2.**

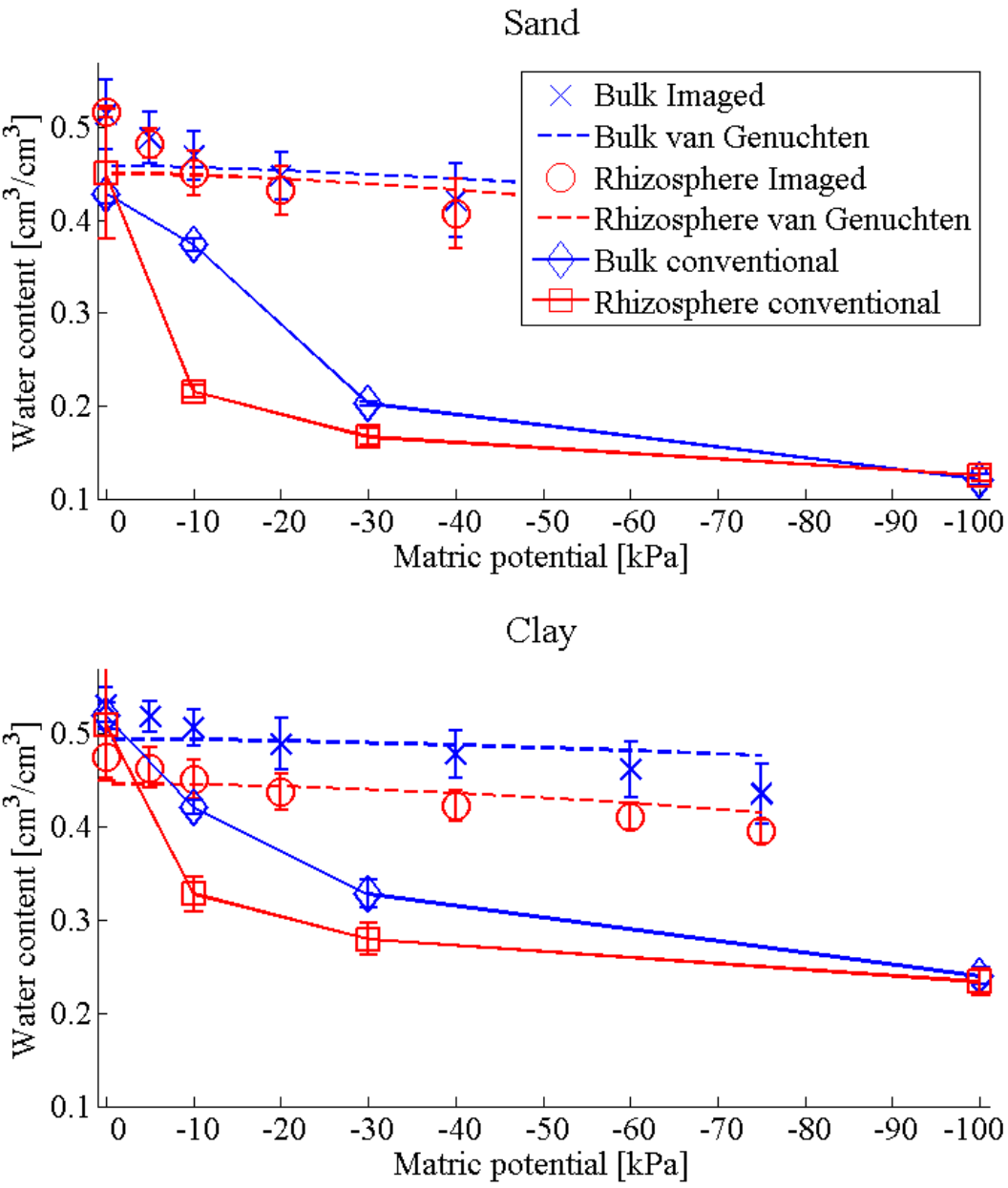

622

623

Figure 3.

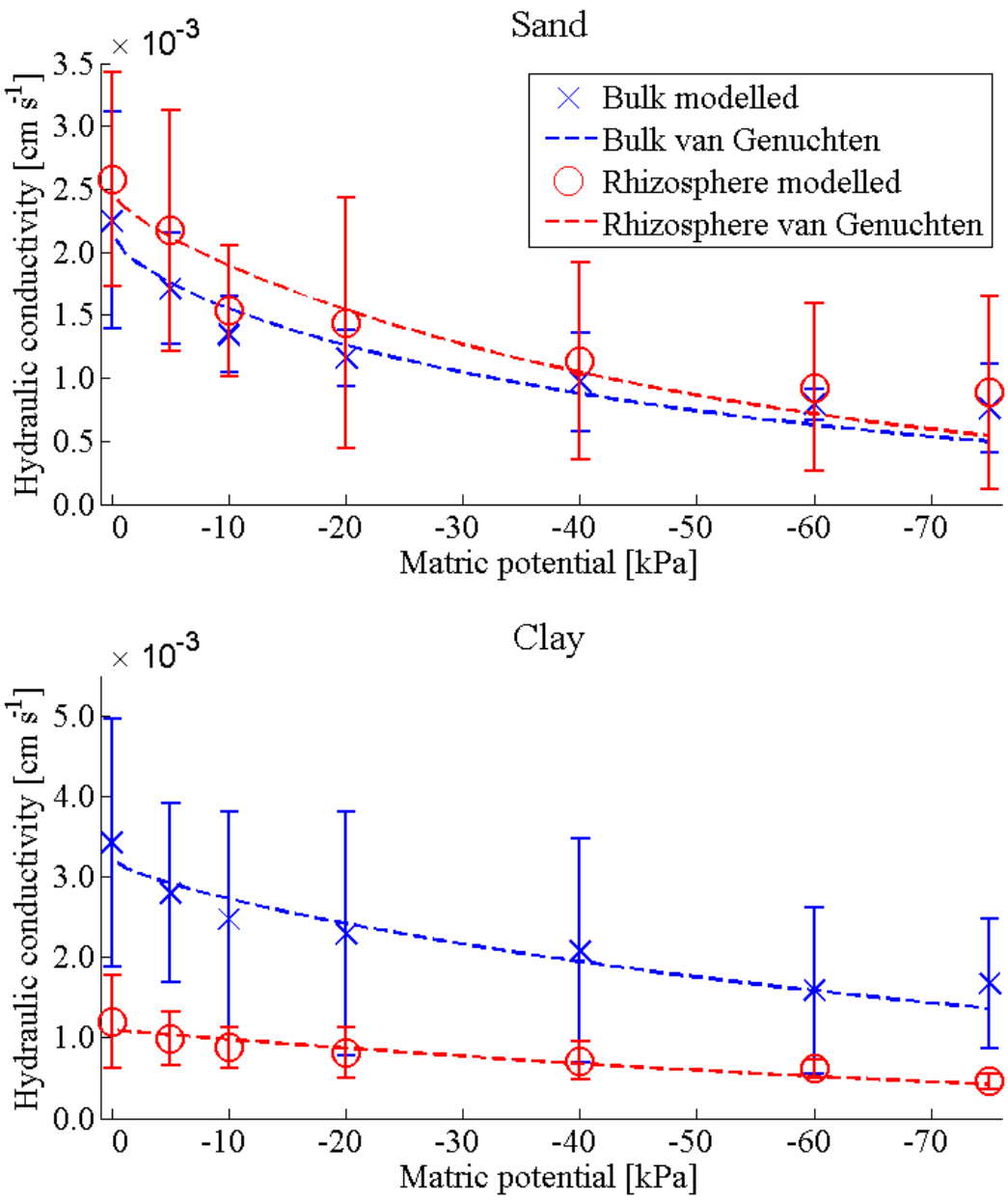
Sand
× 10^-3
Hydraulic conductivity [cm s^-1]
Bulk modelled
Bulk van Genuchten
Rhizosphere modelled
Rhizosphere van Genuchten
Matric potential [kPa]
Clay
× 10^-3
Hydraulic conductivity [cm s^-1]
Matric potential [kPa]

632 **Figure 4.**

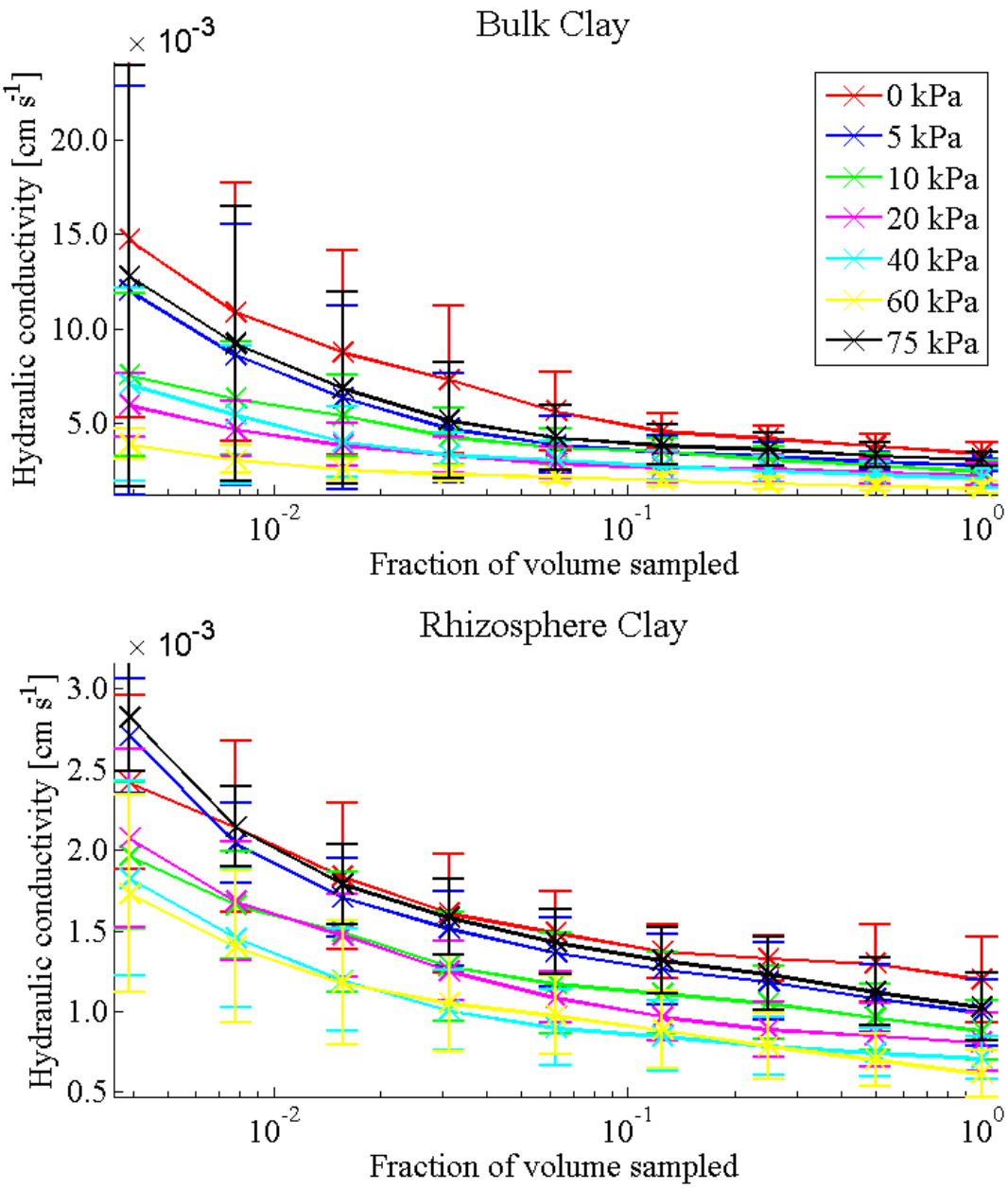

633

634

635

636

637

638

639

Figure 5.

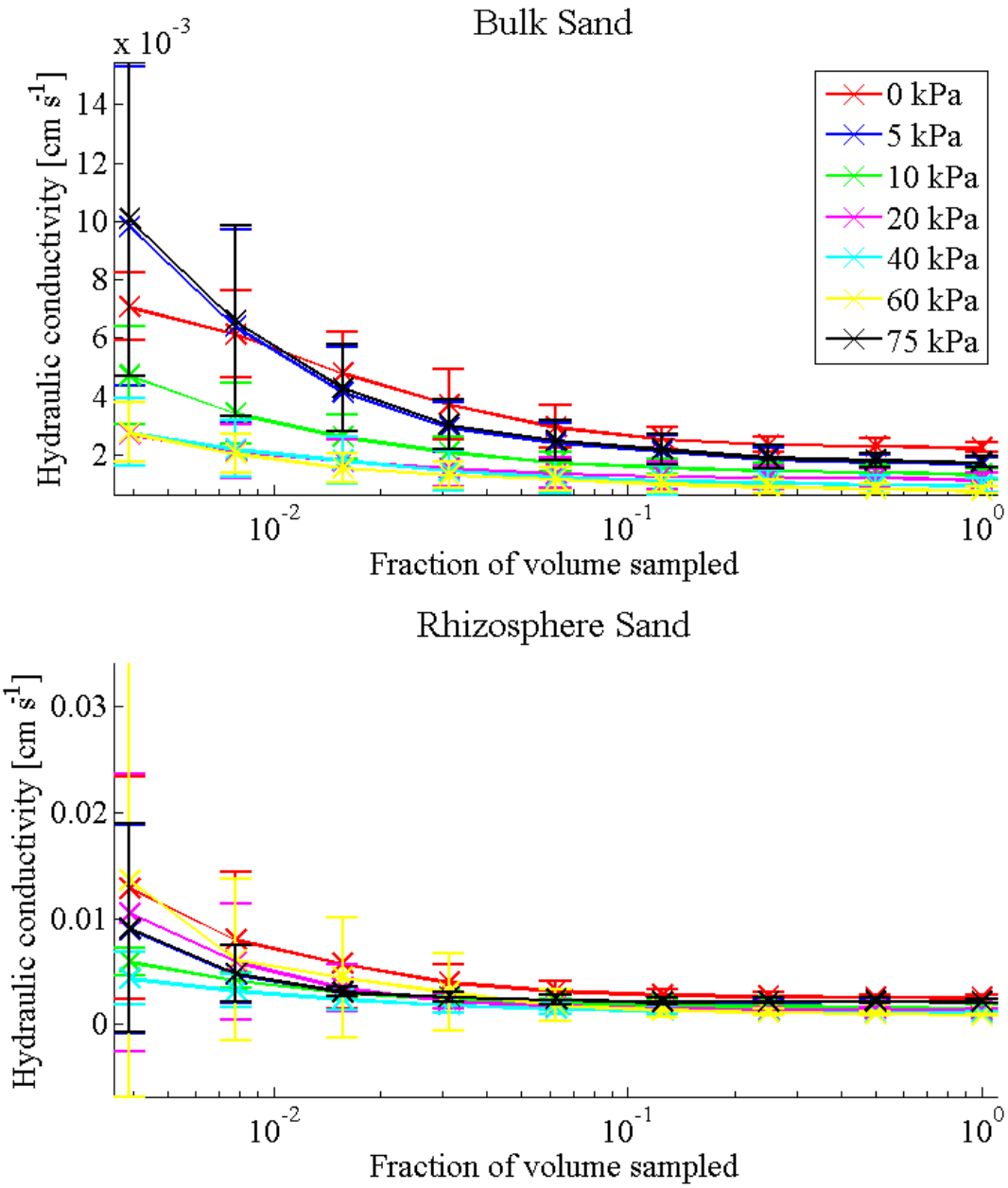
Bulk Sand
x 10^-3
Hydraulic conductivity [cm s^-1]
14
12
10
8
6
4
2
0 kPa
5 kPa
10 kPa
20 kPa
40 kPa
60 kPa
75 kPa
10^-2
10^-1
10^0
Fraction of volume sampled
Rhizosphere Sand
Hydraulic conductivity [cm s^-1]
0.03
0.02
0.01
0
10^-2
10^-1
10^0
Fraction of volume sampled

Figure 6.

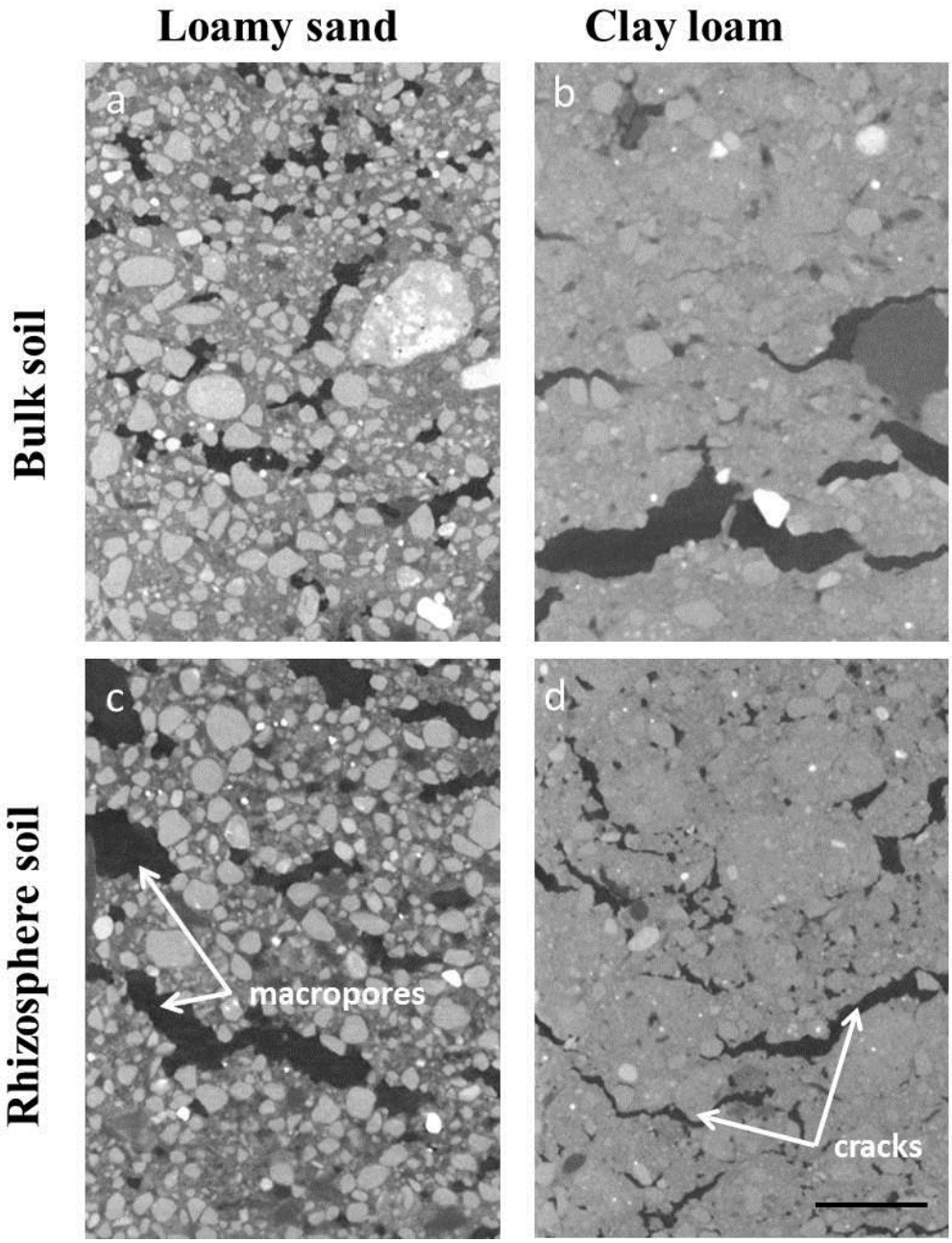
Loamy sand
Clay loam
Bulk soil
Rhizosphere soil
a
b
c
d
macropores
cracks

Figure 7.

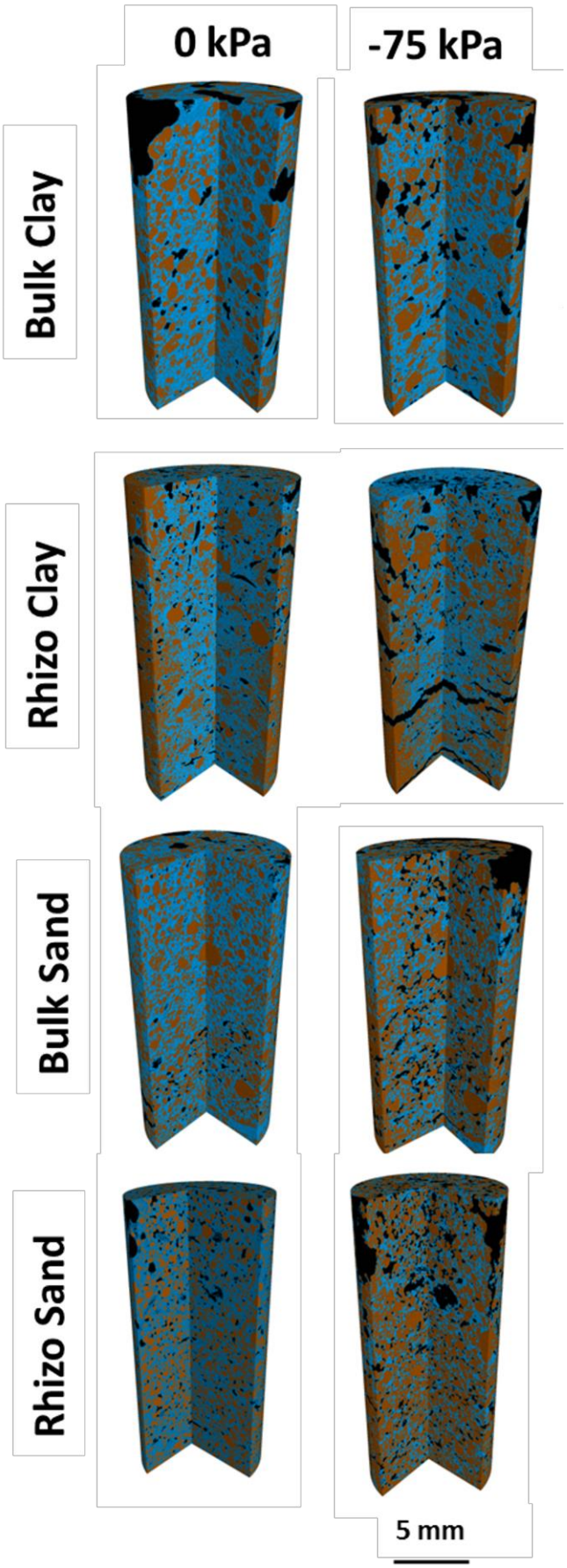

Figure 8.

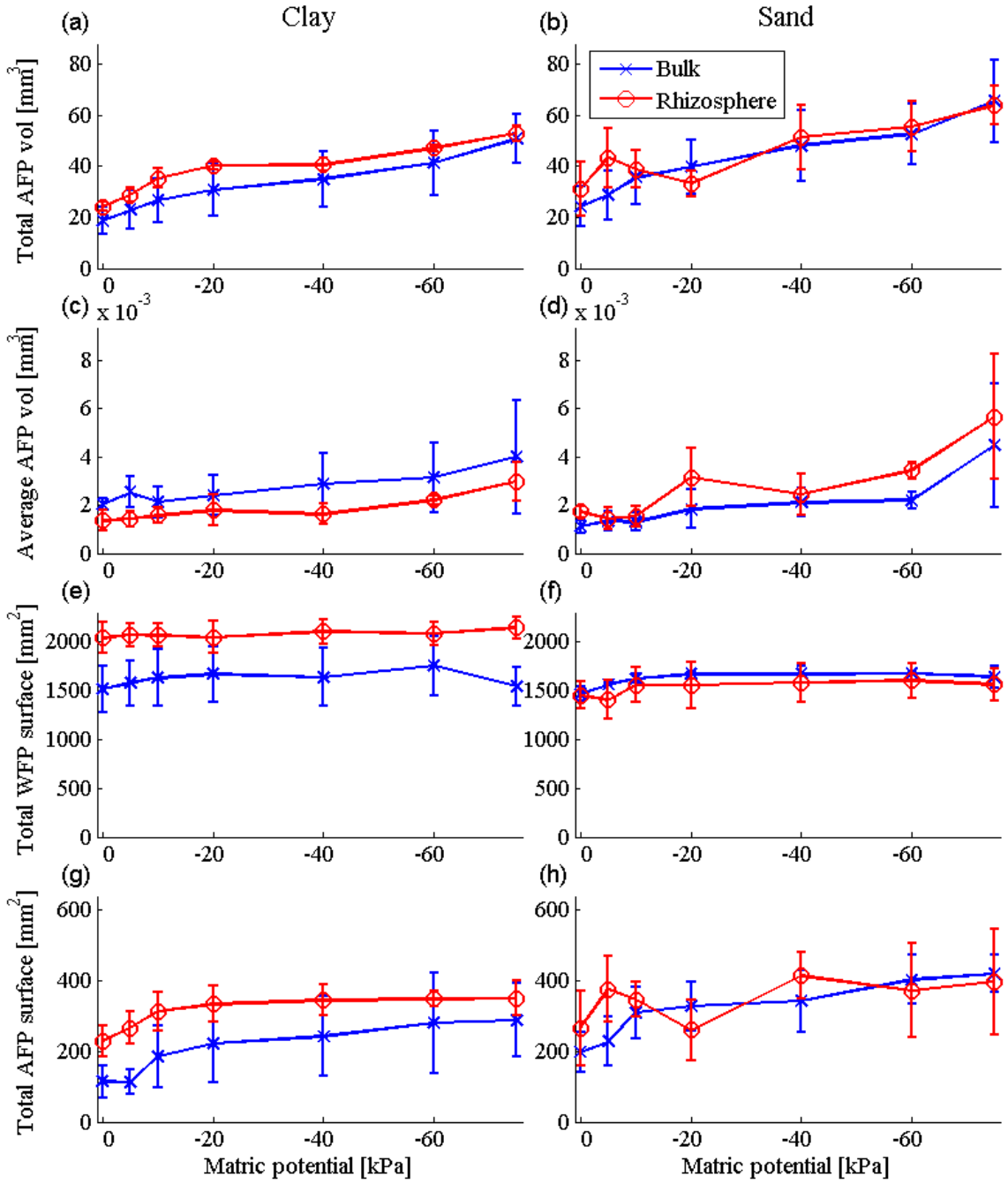
Clay
Sand
(a)
(b)
(c)
(d)
(e)
(f)
(g)
(h)
Bulk
Rhizosphere
Total AFP vol [mm3]
Average AFP vol [mm3]
Total WFP surface [mm2]
Total AFP surface [mm2]
x 10-3
Matric potential [kPa]
Matric potential [kPa]